

# Three-dimensional Optical Tomographic Brain Imaging during Hypercapnia in Rodents

A.Y. Bluestone<sup>a,b</sup>, M. Stewart<sup>c</sup>, J. Lasker<sup>a</sup>, G.S. Abdoulaev<sup>a</sup>, A.H. Hielscher<sup>a</sup>

<sup>a</sup>Columbia University, Depts. of Biomedical Engineering & Radiology New York, NY, 10027  
State University of New York - Downstate Medical Center, Depts. of Pathology<sup>b</sup> and  
Physiology & Pharmacology<sup>c</sup>, Brooklyn, NY, USA 11203

## ABSTRACT

Noninvasive examination of the hemodynamics of brain tissue is of general interest in many areas of medicine and physiology. To date, optical brain studies generate topographic maps, where signals obtained from within the brain are projected onto two-dimensional surface maps. Recently, our group has presented the first three-dimensional, volumetric reconstruction of hemodynamic changes during a Valsalva maneuver in the human forehead. To further validate our three-dimensional diffusion optical tomographic reconstruction algorithm we have turned to experimental studies involving small animals. Here we report on hypercapnia studies performed with 3-month old Sprague-Dawley rats. After anesthetizing the animal a tracheotomy was performed and the rat was artificially respired. The head shaven and secured in a stereotaxic frame an optical probe was positioned between the bregma and lambda skull landmarks. A baseline measurement was recorded and then the inspired gas content was altered. The experimental studies verified the ability of our code to three-dimensionally visualize a global hemodynamic phenomenon in the rat head in response to perturbations in the inspired CO<sub>2</sub> concentrations. Specifically, we incrementally increased the concentration of inspiratory CO<sub>2</sub> (hypercapnia) and visualized the resulting hemodynamic change. We observed a global increase in blood volume and oxygenation, which was consistent with the known physiologic response to hypercapnia. A second set of experiments were designed to determine the sensitivity of the reconstruction to inaccurate probe positioning versus assumed model optrode-position mismatch. We determined that shifts on the order of 1/10 the maximum optrode separation significantly influence the reconstruction and may falsely produce lateralized effects.

**Keywords:** Optical tomography, brain imaging, hypercapnia, small animal model, rodents

## 1. INTRODUCTION

The ability to visualize the vascular changes that accompany neuronal activity represents a key component in the ability to understand the neurophysiology of the brain. Since energy is required for cerebral function, and oxygen delivery can be used as a tag for determining which areas of the brain require energy, an imaging modality that can map the distribution of oxyhemoglobin can potentially map the energy expenditure of the brain. Various noninvasive techniques have been used to interrogate the activation of the cerebral cortex. For example, both positron emission tomography (PET)<sup>1</sup> and functional magnetic resonance imaging (fMRI)<sup>2</sup> observe a significant hemodynamic response at an activated brain region. In fMRI the blood oxygen level dependent (BOLD) signal, resulting from a local change in the paramagnetism of deoxy-hemoglobin, is the basis of mapping functional activation to focal changes in the cerebral blood flow (CBF). In the present study, we use the dynamic near-infrared optical tomographic imager (DYNOT), together with a three-dimensional (3D) iterative image reconstruction algorithm to visualize full tomographic images of regional blood volume, oxygenated hemoglobin, and deoxygenated hemoglobin concentration changes in the same tissue volume. Non-invasive optical imaging systems detect changes in light absorption caused by intrinsic chromophores, the most abundant and hence providing the strongest contrast being hemoglobin.

The work described in this paper was undertaken to assist in the design and validation of a 3D optical tomographic imaging system for small animals. First, we introduce the image reconstruction algorithm. This is followed by a description of the instrumentation and probe design, and a description on how we incorporated anatomical prior knowledge for enhancing our spatial resolution. Finally we investigate the systems utility in-vivo by examining the cerebrovascular response in rats to elevated CO<sub>2</sub> levels (hypercapnia). Under normal conditions, a

mean systemic blood pressure between 60 and 160 mmHg, cardiac output and systemic blood pressure have little effect on the cerebral blood flow due to the brain's ability to autoregulate. Systemic blood pressure doesn't affect CBF, however, carbon dioxide, pH, and oxygen are potent effectors of cerebral vasculature. The response to CO<sub>2</sub> is the largest with a 7% increase in inhaled CO<sub>2</sub> leading to a doubling of the arteriole diameter. The inhalation technique described below is noninvasive, the response can be tightly regulated, provides a fast temporal response to the perturbation and blood pressure doesn't change significantly during the provocation.

## 2. IMAGE RECONSTRUCTION ALGORITHM

For the 3D reconstruction of oxyhemoglobin and deoxygenated hemoglobin in the rat head, we employ in this work a model-based iterative image reconstruction (MOBIIR) scheme. A MOBIIR scheme consists, in general, of three major parts<sup>3</sup>: (1) a forward model that predicts the detector readings (P(r))s based on a given spatial distribution of optical properties ( $\mu_a(r), D(r)$ ) (2) an objective function:

$$\Phi(\mu_a, D) = \left[ \frac{(M - P)}{(M)} \right]^2 \quad (2.1)$$

that compares predicted (P) with measured (M) boundary intensity signals, and (3) an updating scheme that uses the gradient of the objective function with respect to the optical properties to provide a means of updating the optical parameters for subsequent forward calculations. The forward model, which we employ in this study, is the time-independent diffusion equation, given by:

$$-\nabla D \nabla \phi(r) + \mu_a \phi(r) = S(r). \quad (2.2)$$

where the diffusion coefficient  $D = \frac{1}{3\mu_s}$ , and  $\mu_a$  is the absorption coefficient. We incorporated Robin boundary conditions:

$$\phi(r) = 2D(r)R\nabla\phi(r) \quad (2.3)$$

where R is a factor that takes into account the refractive index mismatch between air and tissue (n=1.4, R=2.74). This partial differential equation was solved using a finite element forward solver based on the Galerkin formulation. The solver incorporated a Bramble-Pasciak-Xu (BPX) multi-grid preconditioner and an optimized conjugate gradient matrix solver, and allowed for mesh refinement. The inverse solver used the techniques of adjoint differentiation<sup>4</sup> to calculate the gradient of the objective function with respect to the absorption and scattering coefficients. This gradient was then used to update the optical properties using an iterative conjugate gradient method. Convergence was usually achieved after 10 iterations, requiring ~2 hours on a Linux work station with two 500 Mhz Pentium III processors.

## 3. INSTRUMENTATION

Measurements on the rat head were performed with a dynamic near-infrared optical tomography (DYNOT) instrument<sup>5</sup>. This instrument operates in continuous-wave mode. A beam from each of two laser diodes (wavelength = 760 nm and 830 nm) was sequentially coupled into different fiber optodes, which deliver the laser light to various positions on the rat head. On the target surface, the fibers from the sources and detectors are arranged in a rectangular geometry (Fig. 1). For the measurements presented in this work we used 4 sources and 12 detectors, resulting in 48 source-detector combinations. Three full tomographic data sets, involving all 48 source-detector pairs, were acquired per second. A more detailed description of the device can be found in Schmitz *et al*<sup>5</sup>.

In order to apply the objective function as defined in section 2 towards image reconstruction, one needs to know the absolute measurement values M, which in many cases is difficult to obtain. On the other hand, most of the currently available measurement devices, including our DYNOT system, can provide, with high accuracy, relative measurements ( $M_{\text{pert}}/M_{\text{ref}}$ ), where the two different data sets are acquired during a perturbation ( $M_{\text{pert}}$ ) and reference

state ( $M_{ref}$ ), respectively<sup>6</sup>. To accommodate the data type generated by our instrument we define a modified objective function given by:

$$\Phi = \left[ \frac{\frac{M_{pert}}{M_{ref}} \phi(\mu_a^0, D^0) - \phi(\mu_a^i, D^i)}{\frac{M_{pert}}{M_{ref}} \phi(\mu_a^0, D^0)} \right]^2. \quad (3.1)$$

Here the relative changes ( $M_{pert}/M_{ref}$ ) are multiplied with the calculated detector readings obtained from an initial distribution  $\phi(\mu_a^0, D^0)$  of the optical properties (typically assumed to be homogeneous). In subsequent iterations ( $i$ ) a distribution  $\phi(\mu_a^i, D^i)$  is sought, which produces the same boundary predictions as

$$\frac{M_{pert}}{M_{ref}} \phi(\mu_a^0, D^0). \quad (3.2)$$

The resulting distribution is then a spatial representation of the differences in optical properties that led to the ratio measured between  $M_{pert}$  and  $M_{ref}$ .

To update the initial distribution of optical properties, one must calculate the gradient of the objective function with respect to all optical properties. The calculation of the gradient was performed using the technique of adjoint differentiation as described in a previous publication<sup>4</sup>. The gradient defines a "direction" along which a line minimization is performed. Once the line minimization is completed a new gradient is calculated and a new direction for the line minimization is found within a multidimensional conjugate gradient descent algorithm. Typically 7-15 iterations with different gradients are necessary before the algorithm converges.

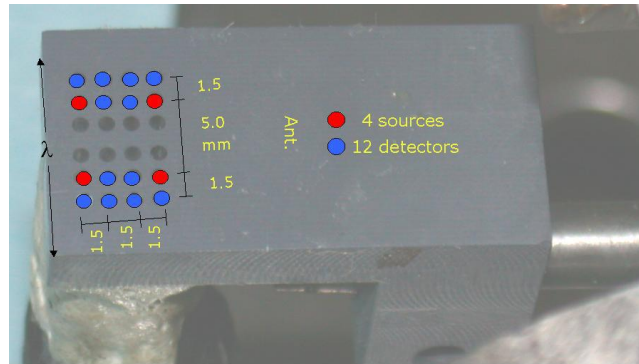


Fig. 1: Optrode probe geometry showing the source-detector locations and alignment with the lambda ( $\lambda$ ) suture line. The animal is placed in the stereotaxic with the dorsal surface facing down.

#### 4. A PRIORI ANATOMICAL MAPS

NIR diffuse optical tomography suffers from an inherently low spatial resolution. Combining the fine structural information that is available from anatomical maps (e.g. obtained with MRI), with the functional information available from NIR imaging promises to enhance the spatial resolution.<sup>7,8</sup> These images may correlate anatomical information with hemoglobin concentration changes and oxygen saturation, as well as other intrinsic chromophores present in tissue. To incorporate this concept of anatomical *a priori* information, we used an atlas of a cryo-sectioned rat cranium<sup>9</sup> to obtain an outline of the skin, skull, brain, and muscle tissue. The rat cranium was chosen since it is a good model for the elucidation of tissue oxygen saturation, ischemia, and other forms of hemodynamic compromise. The two dimensional slices of the rat cranium were translated into a data set that could be used for finite-element-based computation. The finite element 3D mesh was obtained with the skin, brain, bone, and muscle tissues segmented, and then typical optical properties for 800 nm light were assigned to the node locations of the tissues, based on the values from the literature<sup>10</sup>. The node locations were assigned absorption coefficients of  $\mu_a =$

0.2  $\text{cm}^{-1}$  for skin, 0.05  $\text{cm}^{-1}$  for skull, 0.22  $\text{cm}^{-1}$  for muscle, and 0.15  $\text{cm}^{-1}$  for brain, respectively (see Fig. 2). The corresponding reduced scattering coefficients,  $\mu_s'$ , were assigned diffusion coefficients of  $D = c/(3\mu_s') = 1.46 \text{ cm}^2/\text{ns}$  for skin, 0.45  $\text{cm}^2/\text{ns}$  for skull, 0.73  $\text{cm}^2/\text{ns}$  for muscle, and 0.45  $\text{cm}^2/\text{ns}$  for brain, respectively (Fig. 2). This information was incorporated into the model-based iterative image reconstruction algorithm. Specifically, these data sets were employed to model NIR tomography measurements consisting of 4 sources and 12 detectors located on the rat head, 2mm rostral to the lambda suture line.

The reconstruction was initialized with a layered guess assuming a homogenous distribution within each layer (coefficients seen in Fig. 2). The reconstruction algorithm was further constrained by averaging the gradient within each layer except the brain layer before performing an update. Therefore, each of the top three layers moved as a single unit and only the innermost brain layer was allowed to vary over its entire nodal distribution.

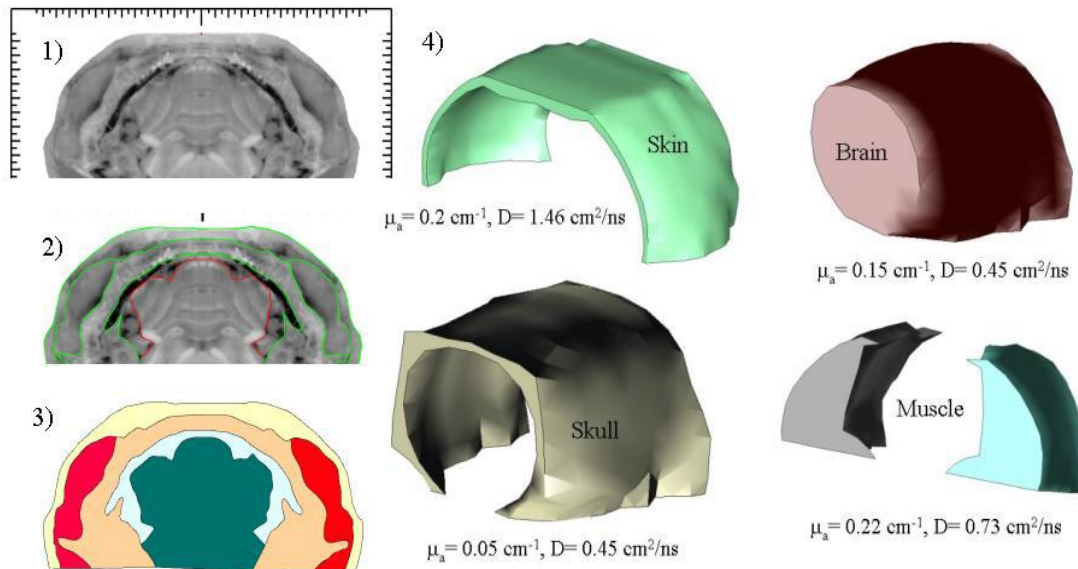


Figure 2: Generating a slice: 1) Cryosection of rat brain 2) Semi-manual extraction of boundaries (green and red) 3) generate splines assign tissue type tags to each layer (skin, muscle, skull, brain) 4) connect multiple coronal sections and generate a 3-d layered mesh. The individual layers are assigned coefficients from the literature.

## 5. ANIMAL PREPARATIONS AND EXPERIMENTAL PROTOCOL

The experiments in this study were designed to look at hemodynamic changes in the forehead of rats induced by changes in the inspiratory concentration of  $\text{CO}_2$ . All experiments and procedures were in accordance with institutional and governmental guidelines. For this study adult male Sprague-Dawley rats, weighing 300-325 g, were initially anesthetized with halothane. Then urethane (1.5mg/kg; 20% in water; ip) was administered as maintenance anesthetic. A polyethylene catheter was placed in the femoral artery and connected to a blood pressure transducer for continuous monitoring of blood pressure (BP). The output of the BP transducer was amplified and digitized. The intra-arterial line was used to draw blood for blood gas analysis. Heart rate was extracted off-line from the BP records. The animal was tracheotomized, and connected to a mechanical ventilator (Harvard Apparatus, South Natick, MA) and respirated at a rate of 65 breaths per minute and a stroke volume of 3cc. After receiving all the implants, the animal was transferred to the modified stereotaxic frame. The skin overlying the dorsal skull was shaved and the optical probe (see Fig. 1) was positioned between the anterior and posterior suture lines; bregma and lambda, respectively. Blood pressure was monitored and recorded continuously for the duration of each experiment. When the arterial blood pressure had stabilized, baseline measurements were recorded and then the relative change during a predefined perturbation (see below) lasting 1-2 minutes was recorded. This was followed by a recovery period lasting at least 10 minutes.

For the hypercapnia experiments described in this study the inspiratory gas content was varied using computer controlled precision flow meters (20 ml for  $\text{CO}_2$ , 1000 ml for  $\text{N}_2$ , 200 ml for  $\text{O}_2$ , Dwyer inc.) which fed into a 350 ml mixing chamber before being released to the ventilator input. Hypercapnia was produced by changing

the fraction of CO<sub>2</sub> to 1.5%, 3%, and 5%. The CO<sub>2</sub> content was varied via a personal computer between 0% and 5%, the O<sub>2</sub> concentration was held fixed at 21%, and the remainder consisting of Nitrogen gas was adjusted to maintain a fixed total flow rate.

An experiment consisted of collecting a minimum of 100 images (3/sec) with 0.3% CO<sub>2</sub> (room air). This was followed by changing the gas concentration for 50-100 seconds, followed by a return to the baseline gas mixture. In Figure 3, a typical signal change observed during a hypercapnia provocation can be seen. The top half of the figure shows the stability of the blood pressure during the extent of the experiment. In the lower half of the figure the timing of the CO<sub>2</sub> perturbation is indicated. For the first 30 seconds a baseline measurement was recorded. At t=30 seconds the concentration of CO<sub>2</sub> was increased to 5% and maintained at that level for 65 seconds. At t=105 the concentration was returned to the baseline level. The measurements attained at detector 12 with a source at position 1 (source-detector separation of 7mm) were used to calculate the changes in oxyhemoglobin (HbO<sub>2</sub>), deoxyhemoglobin (Hb), and total blood volume. One can observe an increase in oxyhemoglobin (red), a decrease in deoxyhemoglobin (blue), and an increase in blood volume (green) during the CO<sub>2</sub> provocation. The delayed onset at t=65 is caused by the delay induced by the mixing chamber and the animals physiologic response. It should be noted that the simultaneous recording of blood pressure (BP) during the experiments eliminated the possibility of the resulting signal change being attributed to perfusion pressure differences.

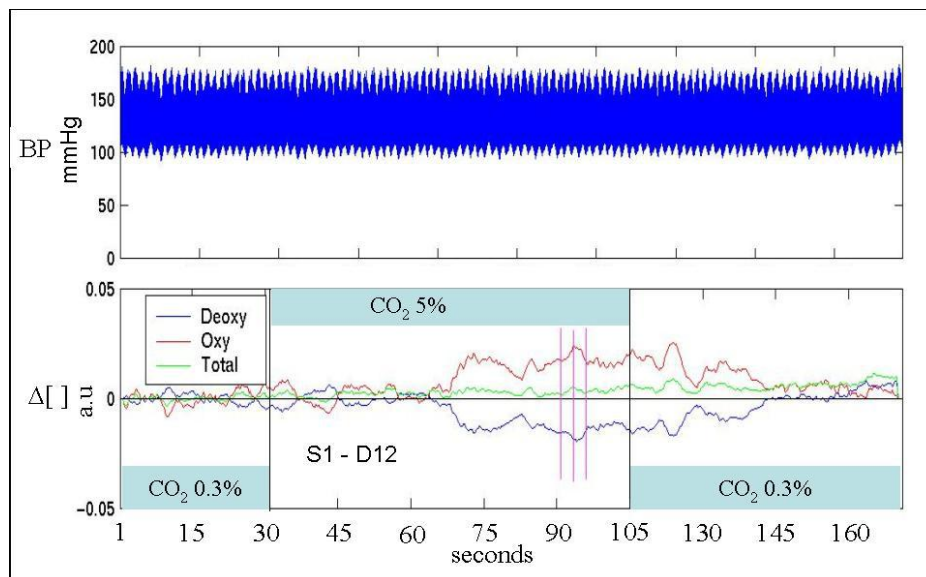


Fig. 3: A typical signal change observed during a hypercapnia provocation. Top half of the figure shows the stability of the blood pressure. The bottom half of the figure shows the change in oxyhemoglobin, deoxyhemoglobin, and blood volume for a single source-detector pair (S1-D12; see also Fig. 4) as well as the timing of the increase in the inspired CO<sub>2</sub> concentration (light blue blocks).

## 6. RESULTS

For the sake of clarity, Fig. 4 depicts the position of the probe relative to the dorsal surface of the rat head. All coronal sections to be presented in this section correspond to the slice located midway between the lambda and bregma suture lines and denoted with an asterisk in the figure. The image reconstruction technique that we employ uses relative measurement data. This means that one can only measure changes from a given baseline. However, as shown in Figs. 5 and 6 one can still make quantitative statements with the regard to these changes.

### 6.1 Dose-response

In this set of experiments the percent of inspired carbon dioxide was increased by fixed amounts of 1.5% 3%, and 5%. At each of these levels, the partial pressure of CO<sub>2</sub> in arterial blood was determined using a blood gas analysis machine. The recorded data increased from a baseline of 45 mmHg (slight hypercapnia) to 56 mmHg at 1.5%, to 66 mmHg at 3%, and 87 mmHg at 5%. The measured partial pressure of oxygen remained constant. Referring to Figure 5, one can see that as the concentration of CO<sub>2</sub> is increased the relative change in oxyhemoglobin (HbO<sub>2</sub>)

increases while deoxyhemoglobin (Hb) decreases. The maximum relative increase in cerebral blood volume (CBV) was about .005 mM from baseline. The maximum relative increase of the oxyhemoglobin concentration was about 0.026 mM, which was similar to the decrease in deoxyhemoglobin concentration (-0.023mM). In Fig. 6 one can see a curvilinear dose response curve, which was generated by selecting a corresponding region of interest in the HbO<sub>2</sub> images from Fig. 5. Here the average HbO<sub>2</sub> concentration in the regions of interest was plotted as a function of CO<sub>2</sub> concentration. All these observation agree with known physiological response to hypercapnia.<sup>11</sup>

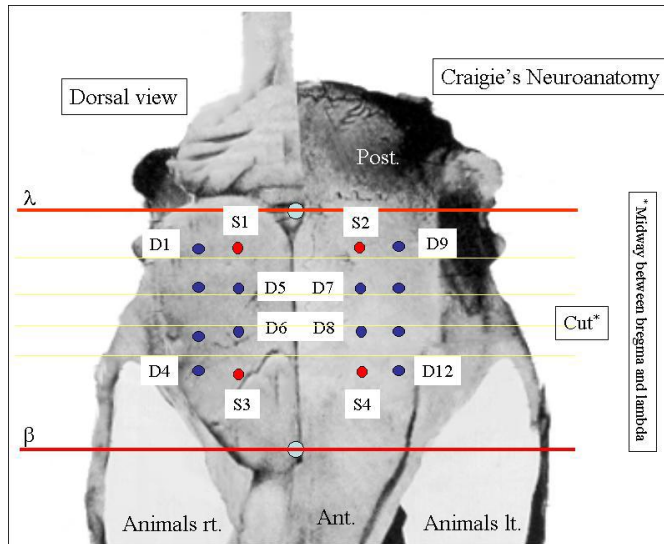


Fig. 4: The optrode locations relative to the dorsal surface of a rat head. The coronal sections in all figures refer to the slice acquired midway between bregma and lambda and denoted by an asterisk.

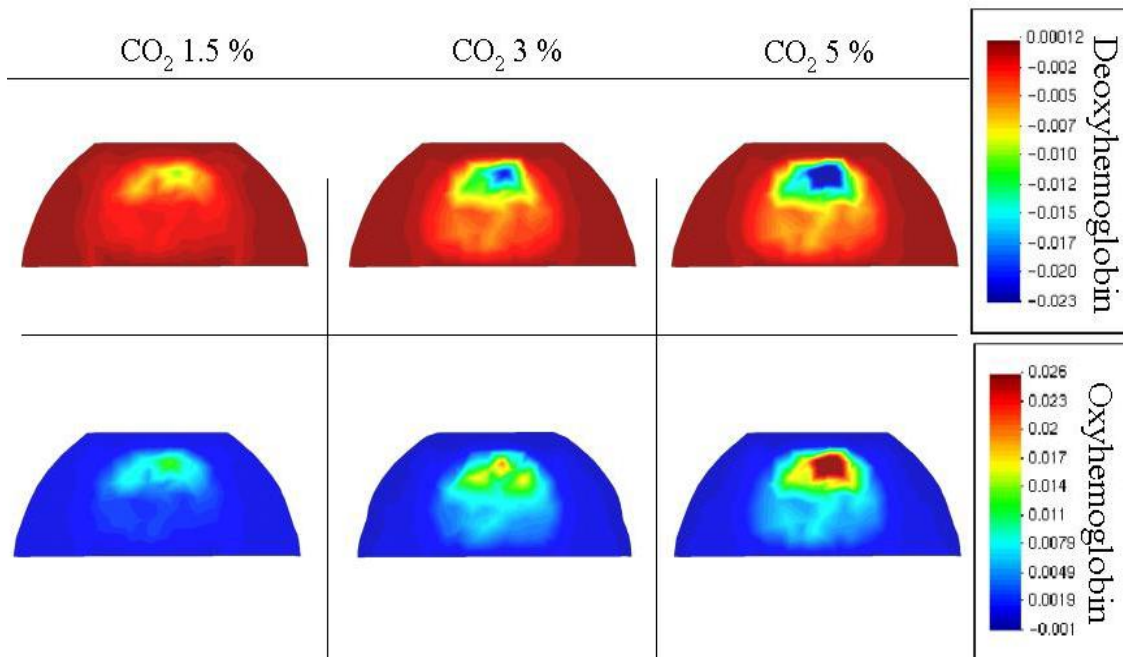


Fig. 5: Dose response for 1.5 % 3 % and 5 % increase in inspired CO<sub>2</sub>. The coronal images are reconstructions of the rat head midway between bregma and lambda suture lines. The top row shows the decrease in deoxyhemoglobin with increasing levels of CO<sub>2</sub>. The middle row shows the increase in oxyhemoglobin, and the bottom row shows the increase in blood volume.

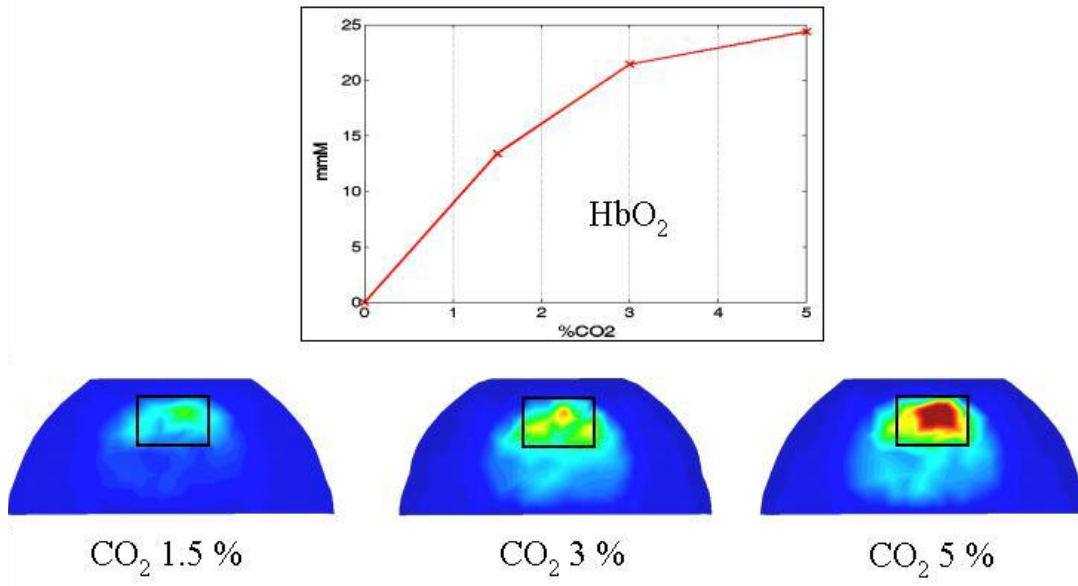


Fig 6: A region of interest (ROI-rectangle) is selected from each image and the average increase in oxyhemoglobin is calculated. The graph plots concentration increase in CO<sub>2</sub> on the x-axis vs. μM increase of oxyhemoglobin on the y-axis.

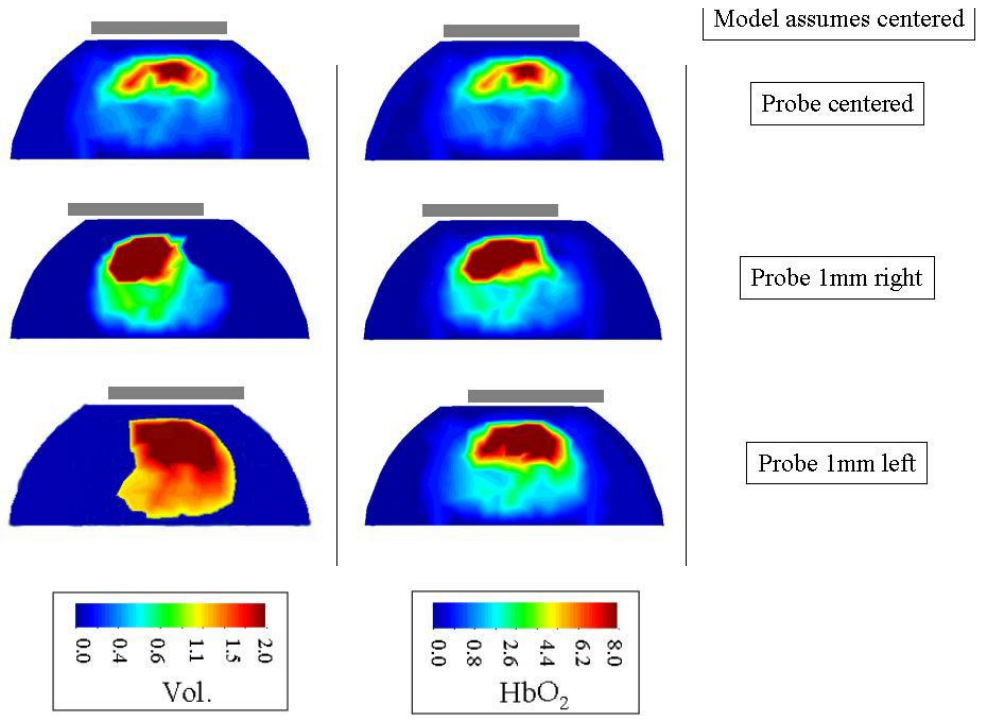


Fig. 7: Coronal sections for the image reconstructions during hypercapnia under various positional shifts of the probe. The first column shows the increase in volume, the second column shows the increase in oxyhemoglobin. In all reconstructions the model assumes the probe is centered. In the top row the model matches the experiment (centered) in the middle row the probe is shifted to the right 1mm. In the bottom row the probe is shifted left 1mm.

## 6.2 Probe positioning

A second set of experiments considered the sensitivity of the reconstruction to inaccuracies in proper positioning of the probe. Specifically, we designed a set of experiments to determine the influence of model-experiment mismatch. In other words, if the model assumes the probe is centered but in the experiment the probe is slightly off-center, how will the reconstruction appear? In order to model this mismatch an accurate means of positioning the probe on the same anatomical landmark was necessary. This was accomplished by modifying a stereotaxic frame to accommodate the optical probe. The frame allowed for the proper securing of the rat via two ear bars and a hook that secured the upper central incisors. The hook was adjustable to allow for level positioning of the rat forehead. The modification to the stereotaxic frame permitted positioning the rat in a supine position with the dorsal surface of the head facing down. By placing the entire optical imaging head on a xyz translater this allowed us to consistently position the edge of the probe in line with the plane formed by the lambda suture line (Fig. 1). Concomitantly, a vertical bar on the imaging head allowed us to position the probe along the midsagittal plane. In the probe positioning experiments the optical probe was shifted using the translater to the left and right of midline by 1.0 mm.

In Figure 7, one can observe three sets of data. In the first row, the probe was centered (gray bar) and the model assumed the probe was centered. As one can see the increase in blood volume is symmetric with respect to the midsagittal plane. In the second row, the probe was shifted to the right but the model assumed the probe was centered. As one can see the increase in blood volume is now pulled to the side of the probe. In the third row, the probe was shifted to the left and the model assumed the probe was centered. In this case one can see that the reconstruction is pulled to the left. As a result of these experiments one can observe that shifts of the probe position, on the order of 1/10 the maximum source-detector separation (1mm), do influence the reconstruction.

## 7. CONCLUSION

We have shown that 3D near-infrared imaging allows for the visualization of the vascular dynamics in the rat brain. The instrument measures oxyhemoglobin, deoxyhemoglobin, and blood volume, simultaneously. Experimentally we observed an increase of 0.005 mM in the total hemoglobin concentration when arterial blood PaCO<sub>2</sub> was raised from 45 mmHg to 87 mmHg with a concurrent increase in oxyhemoglobin of 0.025 mM. The increase in cerebral blood volume (CBV) was found to be present over the entire cortex, and appears to be symmetric with respect to the midsagittal plane (see Fig. 5). Furthermore, unlike MRI, which is only sensitive to deoxyhemoglobin, we have demonstrated the ability of optical tomographic methods to determine relative changes in multiple physiological parameters simultaneously (i.e. oxyhemoglobin, deoxyhemoglobin, and cerebral blood volume). The results obtained here for a model of cerebral vasoreactivity to hypercapnia in a rat are in reasonable agreement with the data from the literature<sup>12</sup>, and offer the potential for further validation with more focal phenomenon.

The second set of experiments considered the sensitivity of the reconstruction to inaccuracies in proper optical probe positioning. The results seem to suggest that shifts in the probe's position, on the order of 1/10 the maximum source-detector separation (1mm), do influence the reconstruction. Therefore, proper probe positioning is essential especially when trying to observe phenomenon that one expects to be lateralized.

## ACKNOWLEDGEMENTS

This work was supported in part by the National Heart, Lung, and Blood Institute (NHLBI-grant #2R44-HL-61057-02A1), and the National Institute of Neurological Disorders and Stroke (NINDS), both part of the National Institutes of Health (NIH), the City of New York Council Speaker's Fund for Biomedical Research: Toward the Science of Patient Care and the Dean's Office of the College of Medicine at the State University of New York (SUNY) Downstate Medical Center in Brooklyn, NY.

## REFERENCES

- <sup>1</sup> M. E. Raichle, Circulatory and metabolic correlates of brain function in normal humans. In: Mountcastle VB, Plum F, Geiger SR (eds) Handbook of physiology- the nervous system. American Physiological Society, Bethesda, pp. 643-674.
- <sup>2</sup> A.L. Baert, K. Sartor, J. E. Youker (eds) Diagnostic Imaging: Functional MRI. Springer-Verlag, Berlin, 2000.
- <sup>3</sup> A.H. Hielscher, A.D. Klose, K.M. Hanson, "Gradient-based iterative image reconstruction scheme for time-resolved optical tomography," IEEE Transactions on medical imaging **18**, pp: 262-271, 1999.

- 
- <sup>4</sup> A.Y. Bluestone, G. Abdoulaev, C.H. Schmitz, R.L. Barbour, A.H. Hielscher, "Three-dimensional optical tomography of hemodynamics in the human head," *Optics Express* **9**, (272-286), 2001.
- <sup>5</sup> C.H. Schmitz, M. Locker, J.M. Lasker, A.H. Hielscher, R.L. Barbour, "Instrumentation for fast functional optical tomography," *Rev. Sci. Instrum.* **73**, (1-11), 2002.
- <sup>6</sup> Y. Pei, H.L. Graber, R.L. Barbour, "Normalized-constraint algorithm for minimizing inter-parameter crosstalk in DC optical tomography," *Optics Express* **9**, (97-109), 2001.
- <sup>7</sup> B. Pogue, K. Paulsen, "High-resolution near-infrared tomographic imaging simulations of the rat cranium by use of a priori magnetic resonance imaging structural information", *Optic Letters* **23**, (1716-1718), 1998.
- <sup>8</sup> A.H. Hielscher and S. Bartel, "Use of penalty terms in gradient-based iterative reconstruction schemes for optical tomography," *Journal of Biomedical Optics* **6**, (183-192), 2001.
- <sup>9</sup> A.W. Toga, E.M. Santori, R. Hazani, K. Ambach, "A 3D digital map of rat brain," *Brain Research Bulletin* **38**, pp: 77-85, 1995. (<http://www.loni.ucla.edu/>)
- <sup>10</sup> A.H. Hielscher, R.E. Alcouffe, R.L. Barbour, "Comparison of finite-difference transport and diffusion calculations for photon migration in homogeneous and heterogeneous tissues," *Physics in Medicine and Biology* **43**, (1285-1302), 1998.
- <sup>11</sup> R.L. Grubb, M.E. Raichle, J.O. Eichling, M.M. Ter-Pogossian, "The effects of changes in PaCO<sub>2</sub> on cerebral blood volume, blood flow, and vascular mean transit time," *Stroke* **5**, (630-639), 1974.
- <sup>12</sup> R. Totaro, G. Barattelli, V. Quaresima, A. Carolei, M. Ferrari, "Evaluation of potential factors affecting the measurement of cerebrovascular reactivity by near-infrared spectroscopy," *Clinical Science* **95**, (497-504), 1998.